Supplementary Table 1. Strains, plasmids and oligonucleotides used in this study.
The table is provided as a separate Excel file.

Supplementary Table 2. Average queuing score (QS) of individual ORFs. QS is calculated as in Kasari *et al.* 2019 (Kasari *et al.*, 2019b) as outlined schematically in Supplemental Figure 2.
The table is provided as a separate Excel file. 5PSeq data analysis performed on pooled data sets from three biological replicates of both wild-type and Δ*new1* strains collected at both 20°C and 30°C.

Supplementary Table 3. Average queuing score (QS) of ORFs sorted by C-terminal amino acid or C-terminal codon.
The table is provided as a separate Excel file. C-terminal codons with greater than two-fold changes in QS are highlighted in yellow.

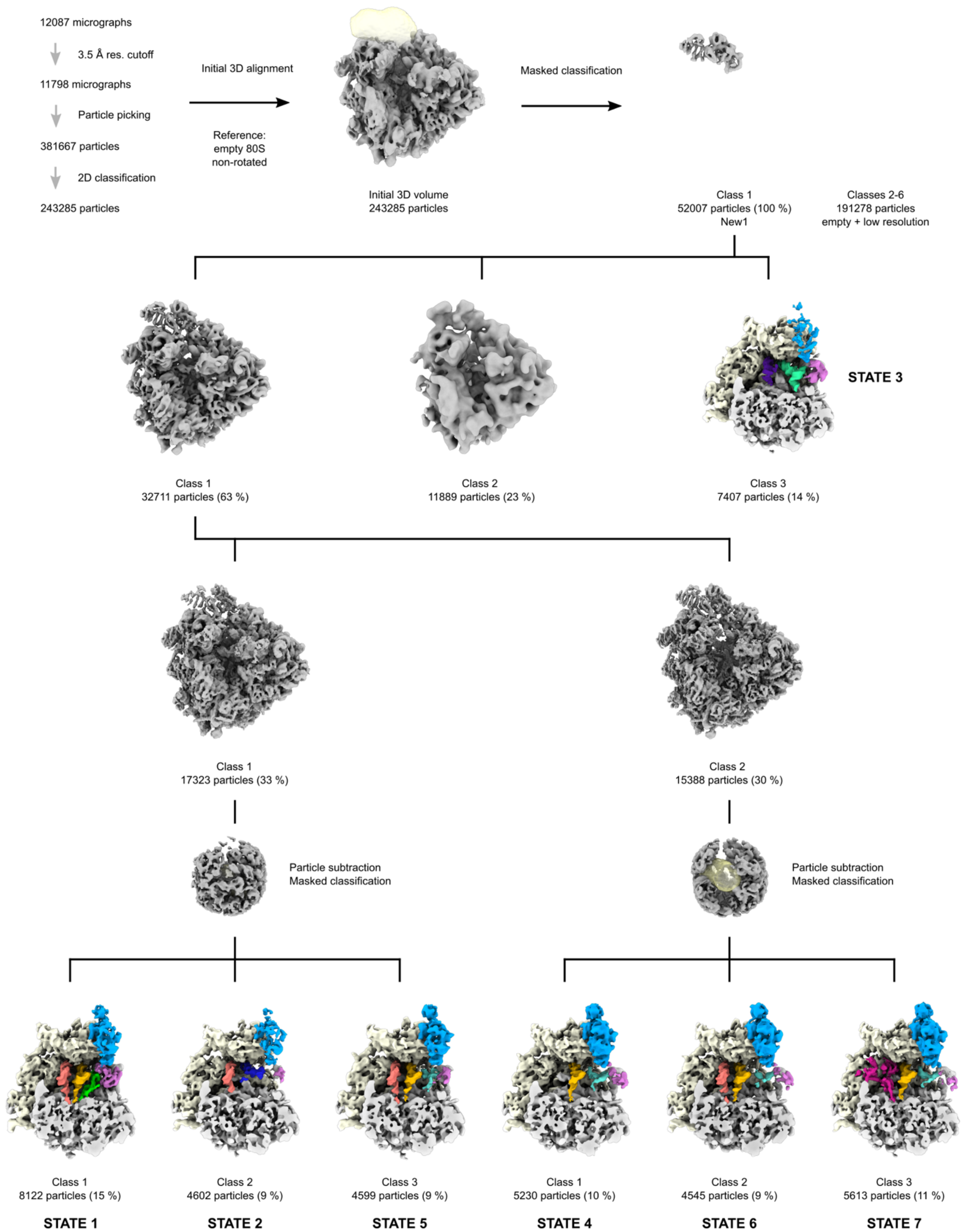

Supplementary Figure 1. Data processing of the *ex vivo* New1p-ribosome complexes.

(**A**) From 12,087 micrographs, 243,285 ribosomal particles were obtained after 2D classification, yielding (**B**) an initial 3D volume, that was (**C**) subjected to masked classification (mask over the New1p area). Classes 2-6 were discarded due to the presence of either vacant ribosomes or low resolution. (**D**) Class 1 was further 3D classified yielding State 3, and (**E-F**) a class (Class 1) that was further 3D classified using particle subtraction to eventually yielded States 1, 2, 4-7.

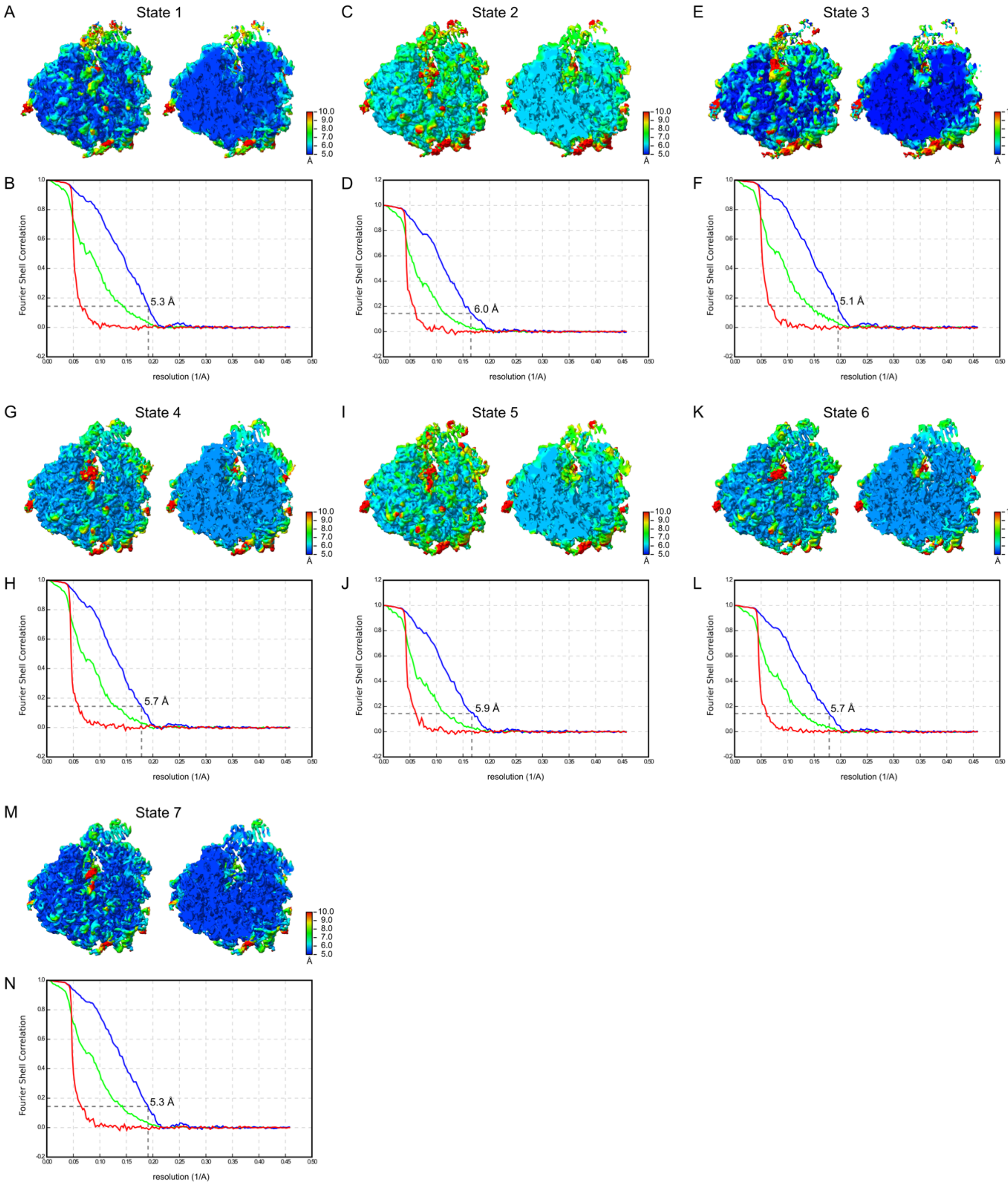

Supplementary Figure 2. Local resolution and Fourier Shell Correlations of States 1-7. (A-M).
Overview (left) and transverse section (right) of the cryo-EM map colored by local resolution is shown with the Fourier Shell Correlation (FSC) curve for (**A-B**) State 1, (**C-D**) State 2, (**E-F**) State 3, (**G-H**) State 4, (**I-J**) State 5, (**K-L**) State 6, and (**M-N**) State 7. The resolution scale for the local resolution is indicated for each state, and the dashed line in the FSC graph at 0.143 indicates the average resolution for each state. The different curves in the FSC graph include the masked map (green), unmasked map (blue), the phase-randomized masked map (red).

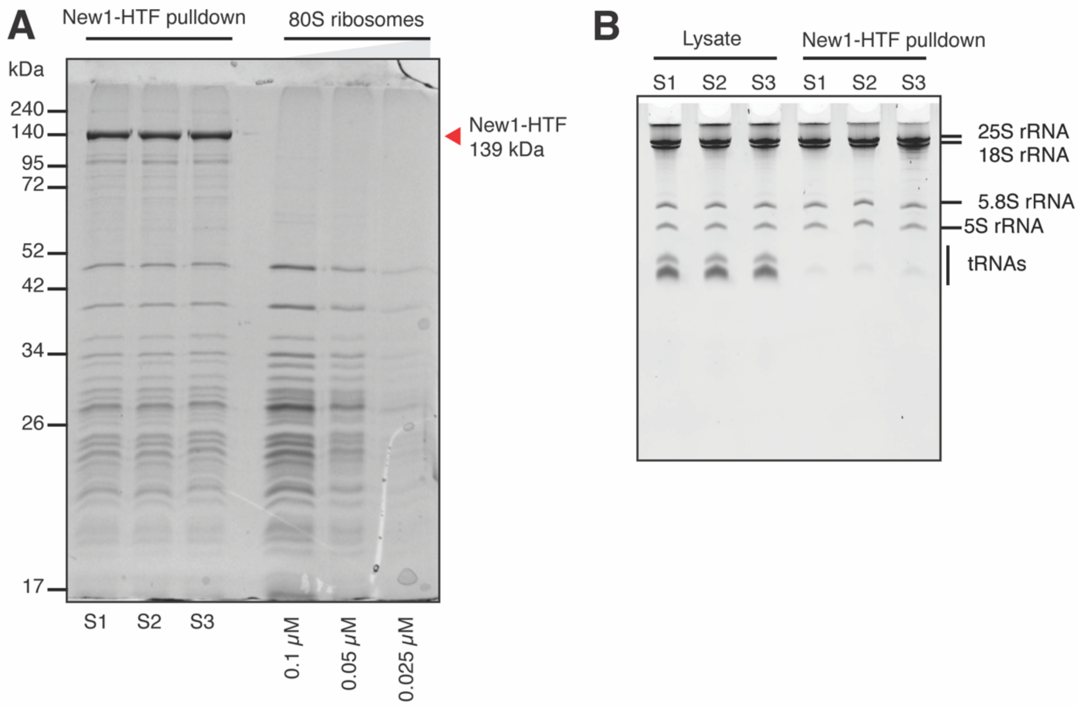

Supplementary Figure 3. Affinity purification of New1-HTF in complex with ribosomes and associated mRNA.

(**A**) Affinity purified samples, in triplicate, from *new1Δ* (VHY68) cells ectopically expressing New1-HTF from VHp911. The cells were grown at 20°C in SC-ura medium and the expression of New1-HTF was induced by supplementing the medium with 2 µM β-estradiol. To identify co-purified ribosomal proteins and to assay ribosomal concentration within the samples, a 2-fold serial dilution of purified *S. cerevisiae* 80S ribosomes were loaded on the gel. The samples were resolved on a 15 % SDS page gel. (**B**) Total RNA was extracted from the input cell lysate and the New1-HTF affinity-purified samples and resolved on a denaturing 8M urea-TBE-acrylamide gel.

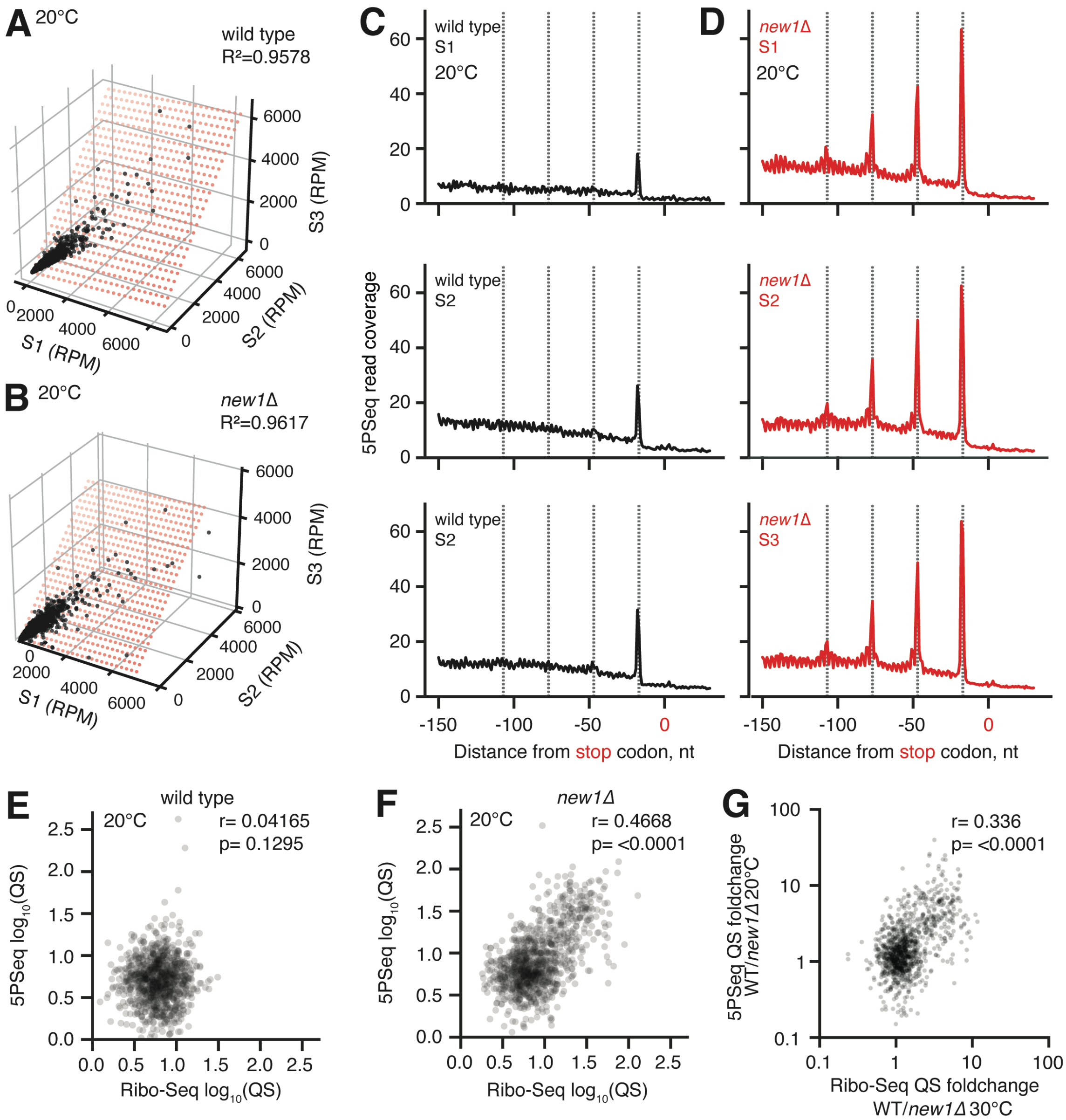

Supplementary Figure 4. **5PSeq data are highly reproducible and are in general agreement with the Ribo-Seq data from Kasari *et al.* 2019 (Kasari *et al.*, 2019b), related to Figure 3.**

(**A**,**B**) Individual ORF read counts (RPM) for individual ORFs for three biological replicates of 5PSeq libraries constructed from wild-type MYJ1171 (A) and *new1Δ* MYJ1173 (B) strains. (**C**,**D**) Metagene analysis of three biological replicas 5PSeq libraries in wild-type (C) and *new1Δ* (D) strains (20°C). (**E**) Comparison of queuing scores (QS) for individual ORFs for pooled 5PSeq (this work) vs Ribo-Seq (Kasari *et al.*, 2019b); both wild-type strain. (**F**) Comparison of pooled 5PSeq and Ribo-Seq derived queuing scores in the wild-type strain. (**G**) QS fold change between wild-type and *new1Δ* strains calculated for 5PSeq and Ribo-Seq datasets. Both 5PSeq and Ribo-Seq analyses were performed on datasets from three biological replicates collected at 20°C.

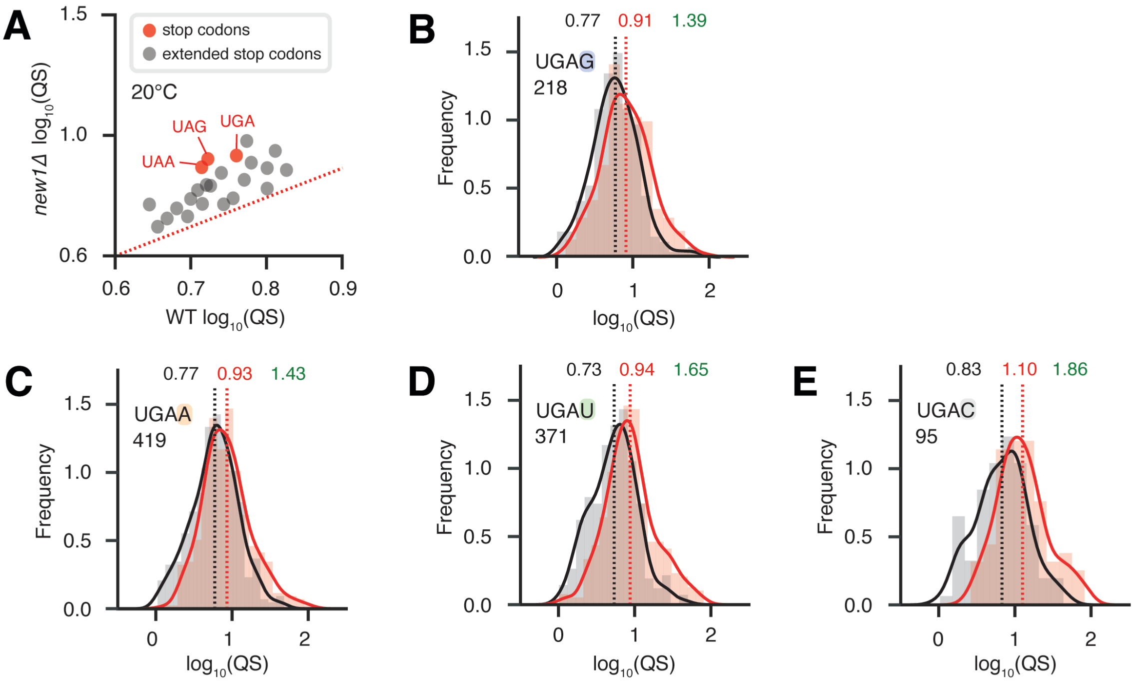

Supplementary Figure 5. New1-dependant ribosomal queuing at the stop codon is not determined by the nature of stop codon 3' context, related to Figure 4.
(**A**) Mean ribosomal queuing score (QS) of ORFs in both the wild-type and *new1Δ* strains, with ORFs parsed by the nature of either extended stop codon (stop codon +1 nt), or just stop codon (grey and red circles, respectively). The red dashed line is a guide for the expected position of data points if there would be no systematic change between in QS between wild type and *new1Δ*. (**B**-**E**) Ribosome queuing score distributions sorted by the nature of the 3' context of the UGA stop codon: (B) UAG G, (C) UAG A, (D) UAG U and (E) UAG C. Geomean QS values in the wild-type and *new1Δ* strains are given in black and red, respectively, and the QS fold change is in green. All analyses were performed on pooled 5PSeq dataset from three replicates collected at 20°C.

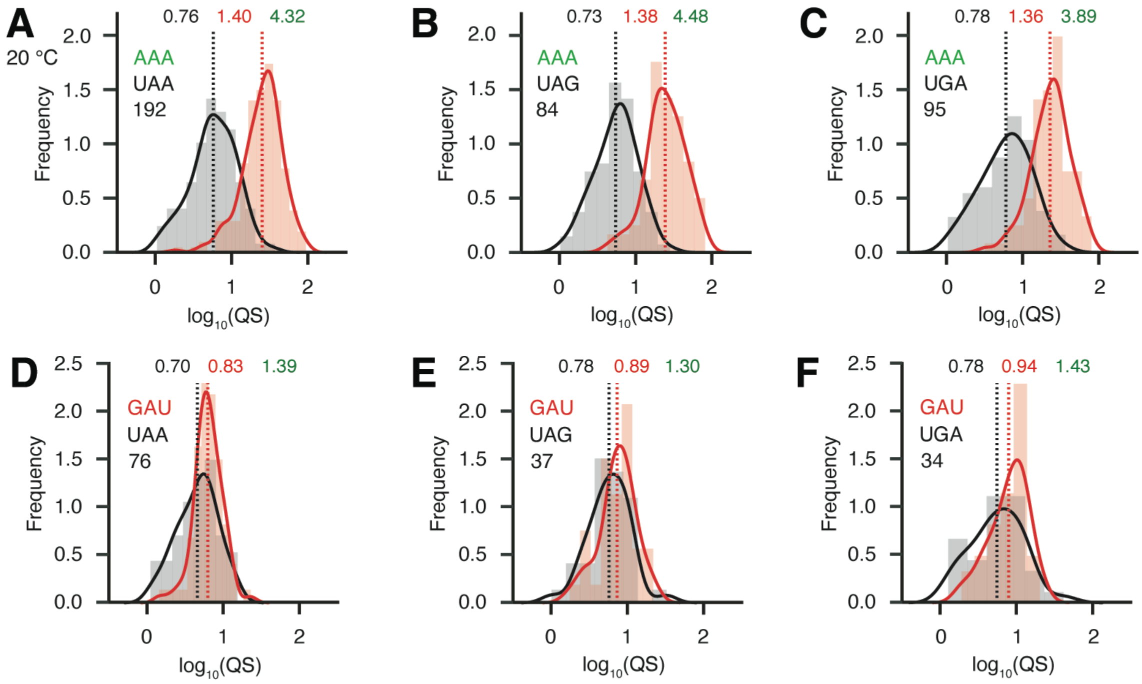

Supplementary Figure 6. Loss of New1 results in ribosomal pile up at C-terminal AAA lysine codons regardless the nature of the stop codon, related to Figure 4. Ribosome queuing score distributions focussing on ORFs parsed by the nature of the C-terminal amino acid [(**A**-**C**) lysine AAA and (**D**-**F**) asparagine GAU codon] as well as the stop codon. The nature of the +4 reside was not taken into account while parsing the data. Number of included ORFs in each analysis is shown on the insert, e.g. the analysis presented on (A) was performed using 192 instances of ORFs encoding UAA preceded by AAA Lys codon. Geomean QS values in the wild-type and *new1Δ* strains are shown in black and red, respectively, and fold change in QS in green. All analysis was performed on pooled 5PSeq dataset from three replicates collected at 20°C.

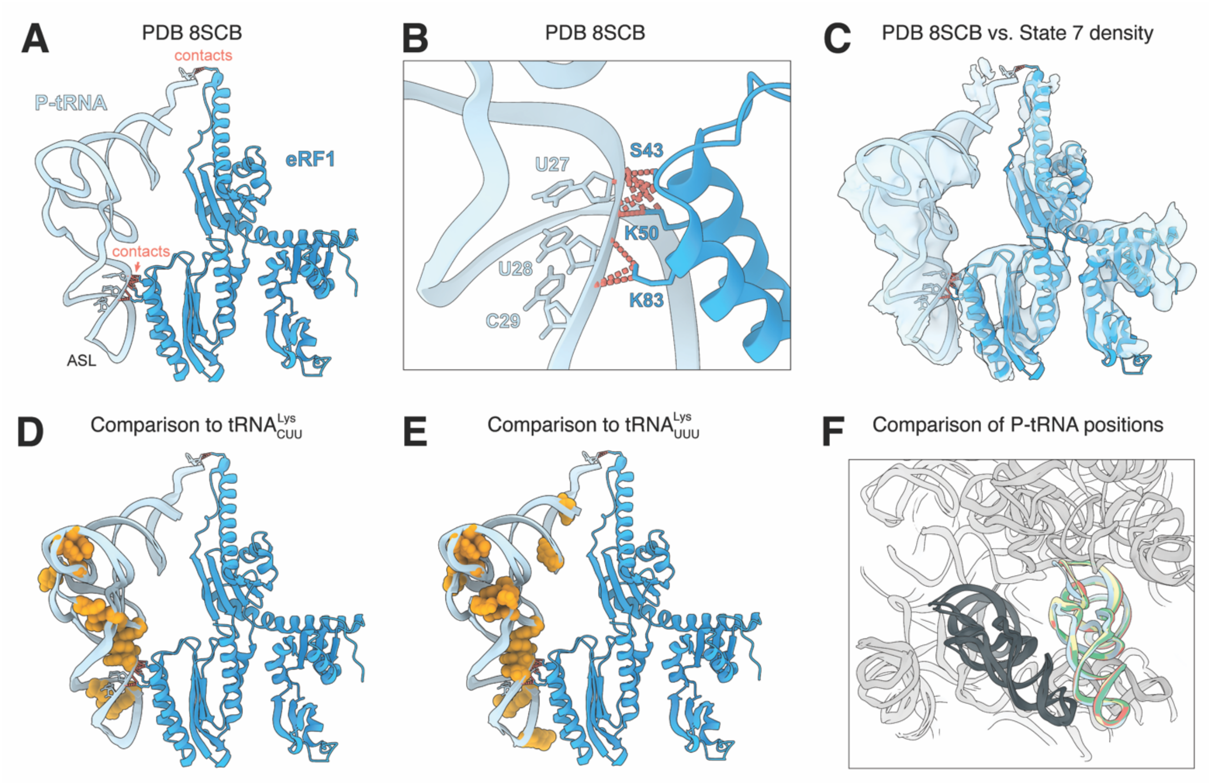

Supplementary Figure 7. Structures of termination complexes.
(**A,B**) Interaction between P-tRNA (cyan) and eRF1 (dark blue) within a mammalian (rabbit) termination complex (PDB ID 8SCB, (Coelho *et al.*, 2024)) with sites of contact indicated by red dashed lines. (**C**) Alignment of P-tRNA and eRF1 from (A) into the cryo-EM density (transparent blue) of State 7 of the New1-termination complex determined here. (**D**,**E**) threading of the sequence and modifications of (D) AAG-decoding tRNA$^{Lys}_{CUU}$ and (E) AAA-decoding tRNA$^{Lys}_{UUU}$ onto the P-tRNA (cyan) of the mammalian (rabbit) termination complex (PDB ID 8SCB, (Coelho *et al.*, 2024)). Orange spheres indicate modifications in the respective tRNAs. (**F**) Alignment of the tRNA^{Lys} [PDB ID 6T83 (Tesina *et al.*, 2020) (yellow) and 6SGC (Chandrasekaran *et al.*, 2019) (cyan)] and tRNA^{Arg} (PDB ID 6T4Q (Tesina *et al.*, 2020) (green) and 6T7I (Tesina *et al.*, 2020) (blue)) onto the mammalian (rabbit) termination complex (PDB ID 8SCB, (Coelho *et al.*, 2024)).